Size of the Localized Electron Emission Sites on a Closed Multiwalled Carbon Nanotube

Erwin C. Heeres,[1] Tjerk H. Oosterkamp,[1] and Niels de Jonge[2,*]

[1]*Leiden Institute of Physics, Leiden University, Niels Bohrweg 2, 2333 CA Leiden, The Netherlands*

[2]*Department of Molecular Physiology and Biophysics, Vanderbilt University School of Medicine, 2215 Garland Avenue, Nashville, Tennessee 37232-0615, USA*

(Received 22 March 2011; published 19 January 2012)

We have measured the size of the localized electron emission sites on multiwalled carbon nanotubes (MWNTs) with caps closed by a fullerenelike structure. MWNTs were individually mounted on tungsten support tips and imaged with a field emission microscope (FEM). The magnification of the FEM was calibrated using electron ray tracing and verified by comparing transmission electron microscope images. The FEM image was also tested for effects of the lateral energy spread. We found ring-shaped emission areas with three flattened sides, of a radius of 1.7 ± 0.3 nm, and separated by 5 ± 1 nm.

DOI: 10.1103/PhysRevLett.108.036804 PACS numbers: 73.63.Fg, 29.25.Bx, 79.70.+q

Electron emission occurs from the apex of a carbon nanotube when placed in an electric field of sufficient strength in vacuum. The resulting electron beam exhibits a specific spatial distribution of electrons [1], reflected in its emission pattern. Several different classes of patterns were found for nanotubes with closed caps and open caps [1–4]. Some groups found a more or less uniform pattern including a few broad spots [3,5]. For certain batches of nanotubes researchers have found a pattern containing typically six ring-shaped emission sites, and lines were observed between these sites. These lines are attributed to interference of electron waves emitted from the spatially separated emission sites [6–8]. The current hypothesis is that the rings in the emission pattern originate from the carbon pentagon rings in the cap [1,4,8–13], with a radius of 1.2 Å [14]. A local electron source of such small size may lead to an extraordinary brightness even to the limit of degeneracy [9,15]. The emission patterns of carbon nanotubes were studied [1,4,8–13] with a field emission microscope (FEM) [16]. But, because the magnification was not known in those experiments it was not possible to verify if the FEM images actually reflected spots of sizes of 1.2 Å. Here, we measure the size of the emission spots with a FEM with a calibrated magnification.

In a FEM, the carbon nanotube mounted on a metal support tip is placed in front of a phosphor screen, and an electric potential U is applied between the tip and the screen, leading to field emission. A magnified image of the emission surface is obtained at the screen on account of the geometric field enhancement at the tip. An important question is thus whether the resolution of the FEM is sufficient to resolve the atomic structure of the cap. The resolution of a FEM δ is given by [16,17]

$$\delta = \sqrt{\sqrt{\frac{2}{m_e e U}}\hbar k R + \frac{4\hbar F k^2 R^2}{\sqrt{2 m_e \phi U}}}, \quad (1)$$

with electron mass m_e, elementary charge e, reduced Planck constant $\hbar$, image compression factor k, emitter radius of curvature R, electric field strength F, and work function φ. For typical values of a multiwalled carbon nanotube (MWNT) electron emitter, $U = 500$ V, $k = 2.5$, and $R = 5$ nm, Eq. (1) gives the FEM resolution $\delta = 1.1$ nm. Thus, the theoretical resolution is not sufficient to resolve an atomic structure.

Figure 1(a) shows a transmission electron microscope (TEM, FEI Tecnai 300 kV) image of the apex of a MWNT with a closed cap of a fullerenelike structure, as produced by the arc-discharge method [18]. The shape of the cap has characteristic flat sides and sharp edges, which are believed to be defined by the locations of the pentagonal carbon rings [19], with each pentagon inducing a local curvature of the otherwise planar structure of hexagonal carbon rings. Figure 1(b) shows a schematic representation of the electron emission sites mapped on the surface of the cap. The main goal of this Letter is to measure the radius of

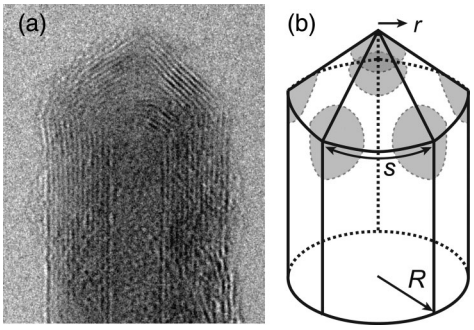

FIG. 1. Multiwalled carbon nanotube (MWNT) with a cap closed by a fullerenelike structure. (a) Transmission electron microscope (TEM) image of a closed MWNT from the sample used in this study. (b) Simplified model of a hemispherically capped carbon nanotube, with local emission sites (gray). Indicated are the size of the emission site r, distance between adjacent emission sites s, and the carbon nanotube radius R.

an emission area (r). We will also determine the distance between the emission sites (s) and the radius of the total emission area including all spots (R), which should match the radius of the nanotube.

MWNTs with closed caps with a fullerenelike structure, and grown by an arc-discharge method (Rosseter) [18,20], were individually mounted on tungsten needles using a nanomanipulator (Omicron) inside a scanning electron microscope (Philips) [21,22]. The adhesion of a nanotube to a tungsten tip was strengthened with the aid of the glue from carbon tape. The nanotube was detached from the bulk sample by careful pulling without breaking it, such that its closed cap remained intact [23]. In Figs. 2(a), 2(b), 2(d), and 2(e) two mounted nanotubes are depicted, referred to as MWNT 1 and MWNT 2, respectively, in the following text. MWNT 1 shows a kink, and it is supported by an additional shorter nanotube from which it protruded; see Fig. 2(a). An image of the closed cap of MWNT 1 is shown in Fig. 2(b). Presumably due to thermal vibrations of the nanotube [24], the image of the cap is somewhat blurred, and its atomic structure cannot be revealed. MWNT 2, see Figs. 2(d) and 2(e), also exhibited a closed cap. The radii, 4.5 ± 0.5 and 5.5 ± 0.5 nm for MWNT 1 and 2, respectively, were measured as FWHM of a line profile through the image of the nanotube perpendicular to its length direction.

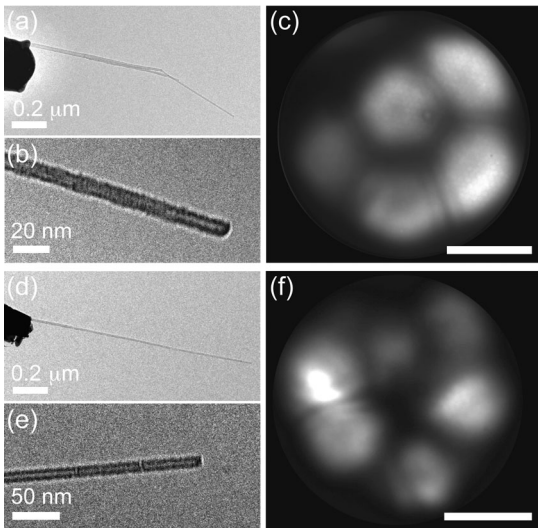

FIG. 2. Microscopy of MWNTs individually mounted on tungsten support tips and used as field emission electron source. (a), (b) TEM images of MWNT 1. (c) Field emission microscope (FEM) image obtained using MWNT 1 placed in front of a phosphor screen and microchannel plate at a distance of 24 mm. An extraction potential of $U = 406$ V was applied between the emitter and the screen, resulting in an emission current of $I = 292$ nA. The tip was heated to ~500 °C. The size of the scale bar equaled 10.5 mm on the original phosphor screen, and represents 5 nm in the FEM image using the calibrated magnification of 2 100 000. (d),(e) TEM images of MWNT 2. (f) FEM image of MWNT 2 obtained at $U = 420$ V, and $I = 102$ nA.

For FEM imaging each nanotube was placed in an ultrahigh vacuum chamber with a base pressure of 1×10^{-10} Torr in front of an imaging device consisting of a microchannel plate and a phosphor screen (Hamamatsu). To clean the nanotube emitter from adsorbed species, it was heated in vacuum for 10 min at a temperature of about 700 °C prior to the experiments. A stable MWNT electron source showed maximal fluctuations of the current of 0.1% [25]. Figure 2(c) shows a FEM image of MWNT 1, with four spots oriented in a half-circle and one spot in their middle. At the top edge of the phosphor screen a sixth spot is faintly visible. The presence of the sixth spot was verified by tilting the MWNT. Thus, the total number of spots equaled the number of pentagon dislocations needed to create a closed cap [26]. Between the two adjacent spots lines can be distinguished that are attributed to interference [6–8].

To relate the emission patterns in Fig. 2(c) to the atomic and electronic structure at the cap of the nanotube we calibrated the magnification of the FEM. This was done by using the equation for the magnification of a field emission microscope $M = z/kR$ [16], with z the tip-screen distance, k the image compression factor, and R the radius of curvature of the emitter. For our carbon nanotube $R = 4.5$ nm as determined from the TEM image, and $z = 24$ mm, but the image compression factor was unknown. Numerical calculations were performed to calculate the magnification of the FEM via ray tracing using Munro's electron beam software.

In order to check the validity of this method the magnification was first determined for a tungsten tip (without MWNT) with a hemispherically shaped apex with a radius of curvature of 100 nm on a tapered shank; see Figs. 3(a) and 3(b). From three different points near the emitter's apex, ray traces were simulated and the landing positions on the screen were obtained and used to calculate the magnification. The magnification was found by comparing the distances between the rays at the screen s_{screen} and at the emitter apex s_{tip}: $M = s_{\text{screen}}/s_{\text{tip}} = 1.4 \times 10^5$. The value $k = 1.5$ is known from literature for a tungsten tip [16], yielding a theoretical value $M_{\text{theor}} = 1.6 \times 10^5$, which corresponds to the value obtained from ray tracing within 15%.

The carbon nanotube field emission tip was modeled as a cylinder with a hemispherically shaped apex on a conically shaped support tip, see Figs. 3(c) and 3(d), and it followed that $M = 2.1 \times 10^6$. Using $M = z/kR$, $k = 2.5$. Based on our TEM image of MWNT 1 we chose to simulate a hemispherical cap model. However, the cap of a carbon nanotube may exhibit sharp edges at the locations of the pentagons of carbon atoms in the cap with an angle of curvature 112.9° [27]. We calculated that the magnification for this geometry was maximal $M = 3.4 \times 10^6$, see Figs. 3(e) and 3(f), but this extreme case occurred only at the locations of the sharp edges. Note that M will likely

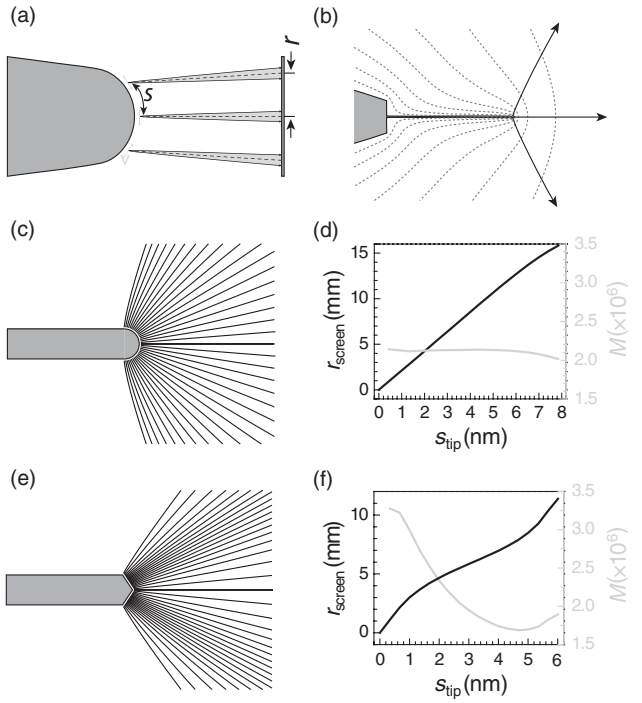

FIG. 3. Geometry used for numerical calculations of the field factor and the magnification (M). Axial symmetry was assumed. (a) Schematic view of a tip in front of an anode (screen). The distance between the starting point of an electron trajectory and the apex of the cap, measured along the surface of the cap, is defined as s_{tip}. The distance from the symmetry axis to the point where the ray hits the screen is defined as r_{screen}. Three points are shown, where the electron ray tracing starts: either with zero transverse velocity (dashed black line) or with nonzero transverse velocity $v_{transverse}$ (solid black lines). The dimensions are not to scale. (b) The MWNT modeled as a cylinder on a support tip. Dotted black lines show equipotential lines and the solid black lines depict three electron trajectories. (c) Ray traces from a MWNT modeled with a hemispherical cap. All traces start with zero transverse energy at 0.5 nm from the apex to simulate the tunneling barrier. (d) Plot of the calculated values of r_{screen} (black, left axis) and M (gray, right axis) as a function of s_{tip}, using the model shown in (c). (e) Ray traces from a MWNT with a pointed cap. (f) r_{screen} and M as a function of s_{tip}, using the model shown in (e).

not be this large in reality due to field penetration, which reduces the extremity of the electric field at the edge.

With the calibrated magnification in Fig. 2(c) we can now determine the values of R, r, and s. To compare the total size of the emission pattern with the diameter of the carbon nanotube we have to realize that the cap is a hemispherical surface that is mapped onto a flat screen. The diameter as measured on the screen d_{screen} corresponds to a distance measured along the surface of the cap with radius R_{FEM}, $d_{screen} = M\pi R_{FEM}$. At the longest side of the emission pattern d_{screen}/M equals 12.8 nm, which translates to a radius of the nanotube of $R_{FEM} = 4.1 \pm 0.6$ nm. This corresponds to the value determined from the TEM image within the error margin. The fact that the value R_{FEM} and the value of R determined from the TEM image of Fig. 2(b) are equal verifies the correct magnification calibration of the field emission microscope.

Values of r were obtained from line profiles through the center of each spot from which FWHM diameter values were calculated ($r = d_{FWHM}/2$) with respect to the minimum (background) intensity in the emission pattern. The individual spots were not exactly round and line profiles were taken over their short sides. Since an individual emission site reflected only a small solid angle of the total cap, a correction in mapping from a curved surface on a flat screen was neglected here. The average value of r of all five spots was 1.7 ± 0.3 nm. The average value of s (the distance between emission sites were corrected for curvature) amounted to 5.3 ± 1.0 nm. The values for MWNT 2 were $M = 1.6 \times 10^6$ (error 15%), $r = 1.6 \pm 0.4$ nm, $s = 4.5 \pm 0.9$ nm, and $R = 6.1 \pm 0.9$ nm.

The distribution of the transverse energy of the transmitted electrons limits the resolution of the FEM. We have deconvolved the FEM image with the point spread function as obtained from the transverse energy distribution to increase the spatial resolution of FEM. The field emission energy distribution of the emitted electron beam was determined by measuring energy spectra of the nanotube emitters using a hemispherical energy analyzer (VSW Atomtech Ltd.). Figure 4(a) shows the energy spectrum of MWNT 1, obtained at $I = 130$ nA and $U = 470$ V. The FEM images and shape of the energy spectrum suggest that the electron emission occurred via field emission. As verification, the current I was measured as a function of U. The plot of $\ln(I/U^2)$ versus $1/U$ was linear, and the field factor $\beta = F/U = (1.7 \pm 0.1) \times 10^7$ m^{-1}, indicating that field emission occurred [16] for the MWNT [28]. The current density as a function of energy can be written as [29]

$$J(E) \propto \frac{\exp(E/d)}{1 + \exp(E/k_B T)}, \tag{2}$$

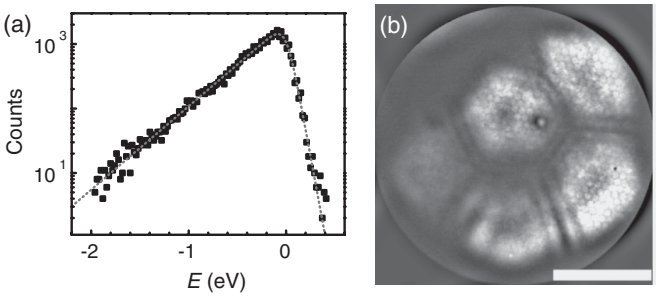

FIG. 4. Deconvolution of the FEM image of MWNT 1. (a) Energy spread measurement of MWNT 1 obtained at 470 V and 130 nA. Dotted gray curve was the theoretical curve of field emission fitted to the data. (b) Deconvolved FEM image obtained using Fig. 2(c). The scale bar represents 5 nm.

where d is the tunneling parameter, k_B the Boltzmann constant, and T the temperature. Equation (2) was fitted to the data, resulting in $d = 0.34$ eV and $T = 601$ K.

The average transverse energy of the emitted electrons is equal to the tunneling parameter d [16,30]. The probability distribution for the transverse energy was obtained by integrating the product of the electron supply function and the transmission coefficient [16] over the normal energy range $(-\infty, 0)$ yielding the transverse energy distribution $D(E_{\text{transverse}})$ [30]:

$$D(E_{\text{transverse}}) \sim e^{-E_{\text{transverse}}/d}, \tag{3}$$

where d is the average value of the transverse energy:

$$\langle E_{\text{transverse}} \rangle = \frac{1}{2m}\langle p_x^2 + p_y^2 \rangle = d. \tag{4}$$

For $U = 470$ V we simulated the electron trajectories for different transverse energies using Munro's electron beam software. The position deviation Δx from the trace of an electron with zero transverse energy was found to be proportional to the square root of the transverse energy, $\Delta x = \alpha\sqrt{E_{\text{transverse}}}$, with the proportionality constant $\alpha = 3.63 \times 10^{-3}$ m$/\sqrt{\text{eV}}$. Substituting this result into Eq. (3) we found that electrons with different transverse energies emitted from a single point on the carbon nanotube cap yield an intensity distribution of electrons on the screen given by

$$D(E_{\text{transverse}}) \sim e^{(\Delta x/\alpha)^2/d}. \tag{5}$$

The Gaussian distribution of Eq. (5) was used as the point spread function to deconvolve the FEM image (using MATLAB). Figure 4(b) shows a much sharper image than Fig. 2(c). The individual emission sites show a dark center. The interference fringes between individual emission sites are more pronounced. Note that the superimposed honeycomb lattice is an artifact of the microchannel plate. The average radius of the emission sites as determined from the FWHMs of the emission patterns in Fig. 4(b) amounts to $r = 1.8 \pm 0.4$ nm, equal to the value determined from the original image within the error margin. Thus, even with the corrected FEM images, the radii of the emission sites are more than a factor of 10 larger than the size of an individual pentagon of carbon atoms.

In conclusion, the emission surface of individual closed MWNT field emission sources was studied with FEM. The calibration of the magnification was verified using the radii of the MWNTs from TEM images. The emission originated from localized sites with $r = 1.7 \pm 0.3$ nm, separated by $s = 5.3 \pm 1.0$ nm on MWNT 1. For MWNT 2 we found $r = 1.6 \pm 0.4$ nm and $s = 4.5 \pm 0.9$ nm. The origin of the emission pattern can be understood as follows. The electron emission from a capped nanotube is known to occur from localized states present at the cap of a nanotube. Electron emission from several localized sites leads to interference of the electron beams, as can be observed as fringes in the emission pattern [7], and these fringes flatten the sides of the spots where they are adjacent [31]. The emission spots show a dark region in their center. From our measurements it does not seem likely that the spots with dark center arise from emission sites of the size of single pentagons in the carbon lattice at the cap. If the emission would have occurred from single pentagons namely, the emission sites would have measured $r = 0.12$ nm. Such small sites would have appeared as small spots in the emission pattern on account of the limited resolution of the FEM, and not as spots with a dark center. The magnification of the FEM may have been enhanced at the sharp edges of a MWNT, but not by more than a factor of 1.6. A localized emission site is an interruption of the delocalized π system of the graphene lattice at the position of one of the bends in the structure needed to form the cap. The site extends over multiple carbon rings [32,33]. It is possible that local field penetration occurs, once electron emission starts, because the electron supply might be limited at interruptions of the electronic structure [34].

We thank Monja Kaiser for the TEM imaging and Jonathan Jarvis and Charles Brau for discussion. This research was supported by FEI Company, the Dutch Ministry of Economic Affairs, and the U.S. Office of Naval Research (No. 10212689).

*Current address: INM—Leibniz-Institut für Neue Materialien gGmbH, Campus D2 2, D-66123 Saarbrücken, Germany.
niels.dejonge@inm-gmbh.de

[1] Y. Saito, K. Hata, and T. Murata, Jpn. J. Appl. Phys. **39**, L271 (2000).
[2] Y. Saito, K. Hamaguchi, K. Hata, K. Uchida, Y. Tasaka, F. Ikazaki, M. Yumura, A. Kasuya, and Y. Nishina, Nature (London) **389**, 554 (1997).
[3] N. de Jonge, M. Doytcheva, M. Allioux, M. Kaiser, S. A. M. Mentink, K. B. K. Teo, R. G. Lacerda, and W. I. Milne, Adv. Mater. **17**, 451 (2005).
[4] Y. Saito, Y. Tsujimoto, A. Koshio, and F. Kokai, Appl. Phys. Lett. **90**, 213108 (2007).
[5] K. A. Dean and B. R. Chalamala, J. Vac. Sci. Technol. B **21**, 868 (2003).
[6] C. Oshima, K. Mastuda, T. Kona, Y. Mogami, M. Komaki, Y. Murata, T. Yamashita, T. Kuzumaki, and Y. Horiike, Phys. Rev. Lett. **88**, 038301 (2002).
[7] K. Hata, A. Takakura, K. Miura, A. Ohshita, and Y. Saito, J. Vac. Sci. Technol. B **22**, 1312 (2004).
[8] G. L. Martin and P. R. Schwoebel, Surf. Sci. **601**, 1521 (2007).
[9] K. Hata, A. Takakura, A. Ohshita, and Y. Saito, Surf. Interface Anal. **36**, 506 (2004).
[10] T. Yamashita, K. Mastuda, T. Kona, Y. Mogami, M. Komaki, Y. Murata, C. Oshima, T. Kuzumaki, and Y. Horiike, Surf. Sci. **514**, 283 (2002).

[11] M. Khazaei, K. A. Dean, A. A. Farajian, and Y. Kawazoe, J. Phys. Chem. C **111**, 6690 (2007).
[12] T. Fujieda, M. Okai, and H. Tokumoto, Jpn. J. Appl. Phys. **47**, 2021 (2008).
[13] T. Fujieda, K. Hidaka, M. Hayashibara, T. Kamino, H. Matsumoto, Y. Ose, H. Abe, T. Shimizu, and H. Tokumoto, Appl. Phys. Lett. **85**, 5739 (2004).
[14] K. Hedberg, L. Hedberg, D. S. Bethune, C. A. Brown, H. C. Dorn, R. D. Johnson, and M. De Vries, Science **254**, 410 (1991).
[15] J. D. Jarvis, H. L. Andrews, B. Ivanov, C. L. Stewart, N. de Jonge, E. C. Heeres, W. P. Kang, Y. M. Wong, J. L. Davidson, and C. A. Brau, J. Appl. Phys. **108**, 094322 (2010).
[16] R. H. Good and E. W. Müller, *Handbuch Der Physik, XXI* (Springer Verlag, Berlin, 1956).
[17] The original equation by R. H. Good and E. W. Müller [16] lacks a factor of 2 in the transverse energy part of the broadening, which has been corrected for.
[18] V. A. Ryzhkov, Physica (Amsterdam) **323B**, 324 (2002).
[19] S. Iijima, Mater. Sci. Eng. B **19**, 172 (1993).
[20] V. A. Ryzhkov, European Patent Application 7244408, 2007).
[21] J. H. Hafner, C.-L. Cheung, T. H. Oosterkamp, and C. M. Lieber, J. Phys. Chem. B **105**, 743 (2001).
[22] N. de Jonge, Y. Lamy, and M. Kaiser, Nano Lett. **3**, 1621 (2003).
[23] E. C. Heeres, A. J. Katan, M. H. van Es, A. F. Beker, M. Hesselberth, D. J. van der Zalm, and T. H. Oosterkamp, Rev. Sci. Instrum. **81**, 023704 (2010).
[24] M. M. J. Treacy, T. W. Ebbesen, and J. M. Gibson, Nature (London) **381**, 678 (1996).
[25] N. de Jonge, M. Allioux, J. T. Oostveen, K. B. K. Teo, and W. I. Milne, Appl. Phys. Lett. **87**, 133118 (2005).
[26] S. lijima, T. Ichihashi, and Y. Ando, Nature (London) **356**, 776 (1992).
[27] S. N. Naess, A. Elgsaeter, G. Helgesen, and K. D. Knudsen, Sci. Tech. Adv. Mater. **10**, 065002 (2009).
[28] N. de Jonge, M. Allioux, M. Doytcheva, M. Kaiser, K. B. K. Teo, R. G. Lacerda, and W. I. Milne, Appl. Phys. Lett. **85**, 1607 (2004).
[29] N. de Jonge, M. Allioux, J. T. Oostveen, K. B. K. Teo, and W. I. Milne, Phys. Rev. Lett. **94**, 186807 (2005).
[30] P. W. Hawkes and E. Kasper, *Principles of Electron Optics* (Academic, London, 1996).
[31] P. Kruit, M. Bezuijen, and J. E. Barth, J. Appl. Phys. **99**, 024315 (2006).
[32] A. Buldum and J. P. Lu, Phys. Rev. Lett. **91**, 236801 (2003).
[33] A. De Vita, J. C. Charlier, X. Blase, and R. Car, Appl. Phys. A **68**, 283 (1999).
[34] J. Peng, Z. Li, C. He, G. Chen, W. Wang, S. Deng, N. Xu, X. Zheng, G. Chen, C. J. Edgcombe, and R. G. Forbes, J. Appl. Phys. **104**, 014310 (2008).